ACS APPLIED MATERIALS & INTERFACES

www.acsami.org

Research Article

Electrochemically Exfoliated Platinum Dichalcogenide Atomic Layers for High-Performance Air-Stable Infrared Photodetectors

Yaping Ma, Xiji Shao, Jing Li,* Bowei Dong, Zhenliang Hu, Qiulan Zhou, Haomin Xu, Xiaoxu Zhao, Hanyan Fang, Xinzhe Li, Zejun Li, Jing Wu, Meng Zhao, Stephen John Pennycook, Chorng Haur Sow, Chengkuo Lee, Yu Lin Zhong, Junpeng Lu, Mengning Ding, Kedong Wang,* Ying Li,* and Jiong Lu*

Cite This: *ACS Appl. Mater. Interfaces* 2021, 13, 8518–8527

Read Online

ACCESS | Metrics & More | Article Recommendations | Supporting Information

ABSTRACT: Platinum dichalcogenide (PtX_2), an emergent group-10 transition metal dichalcogenide (TMD) has shown great potential in infrared photonic and optoelectronic applications due to its layer-dependent electronic structure with potentially suitable bandgap. However, a scalable synthesis of $PtSe_2$ and $PtTe_2$ atomic layers with controlled thickness still represents a major challenge in this field because of the strong interlayer interactions. Herein, we develop a facile cathodic exfoliation approach for the synthesis of solution-processable high-quality $PtSe_2$ and $PtTe_2$ atomic layers for high-performance infrared (IR) photodetection. As-exfoliated $PtSe_2$ and $PtTe_2$ bilayer exhibit an excellent photoresponsivity of 72 and 1620 mA W^{-1} at zero gate voltage under a 1540 nm laser illumination, respectively, approximately several orders of magnitude higher than that of the majority of IR photodetectors based on graphene, TMDs, and black phosphorus. In addition, our $PtSe_2$ and $PtTe_2$ bilayer device also shows a decent specific detectivity of beyond 10^9 Jones with remarkable air-stability (>several months), outperforming the mechanically exfoliated counterparts under the laser illumination with a similar wavelength. Moreover, a high yield of $PtSe_2$ and $PtTe_2$ atomic layers dispersed in solution also allows for a facile fabrication of air-stable wafer-scale IR photodetector. This work demonstrates a new route for the synthesis of solution-processable layered materials with the narrow bandgap for the infrared optoelectronic applications.

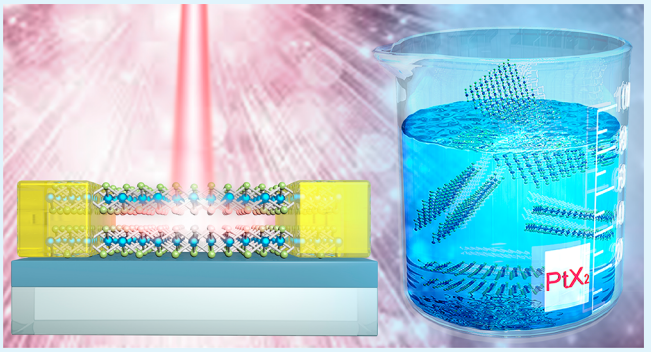

KEYWORDS: *IR photodetectors, electrochemical exfoliation, bilayer $PtSe_2$, bilayer $PtTe_2$, air-stable*

INTRODUCTION

Two-dimensional (2D) layered semiconductors have demonstrated great potential in future photonic and optoelectronic applications due to their flexible atomically thin structures and outstanding layer-dependent electronic and optical properties.[1−6] In particular, infrared (IR) photodetectors have been widely used in remote sensing, optical communications, and IR imaging.[7] Therefore, tremendous efforts have been devoted to search for promising 2D candidates for IR photodetection with high photoresponsivity and specific detectivity including graphene,[8−12] TMD,[13−16] and black phosphorus (BP).[17−20] For example, it has been reported that graphene exhibits an ultrawide band detection because of its semimetallic nature. Unfortunately, the photodetection performance of graphene is limited largely by its low absorption coefficient and short lifetime of the photogenerated carriers.[11,21,22] Alternatively, engineering graphene-based heterostructures has been exploited to further enhance the performance of graphene-based photodetection.[23] In contrast, semiconducting TMDs with sizable bandgaps and strong absorption at specific wavelengths are considered as appealing alternatives beyond graphene for photodetection. To date, most reports focus on the exploration of group-6 TMDs with bandgaps ranging between 1 and 2.5 eV, and thus their optoelectronic devices mainly work in the visible light regime.[24−26] In addition to TMDs, BP with a high carrier mobility demonstrates layer-dependent direct bandgaps ranging from the visible to infrared regime, which has sparked enormous research interest in the photodetection in near and mid-IR range. However, the extreme air-sensitivity of BP poses a formidable challenge for its practical application under ambient conditions.[19,20] Therefore, the development of new approaches for the synthesis of air-stable 2D semiconductors with suitable narrow bandgap for the infrared optoelectronic and photonic applications is highly desired.

Received: November 17, 2020
Accepted: February 2, 2021
Published: February 11, 2021

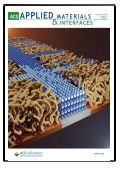

https://dx.doi.org/10.1021/acsami.0c20535
ACS Appl. Mater. Interfaces 2021, 13, 8518–8527

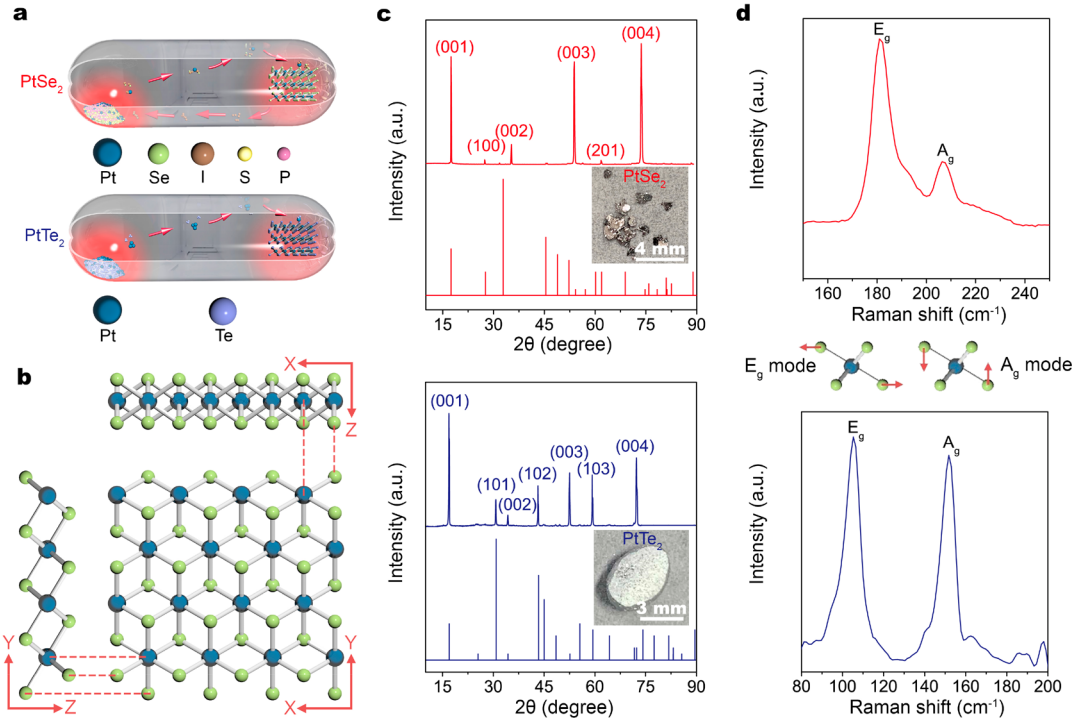

Figure 1. Synthesis of $PtSe_2/PtTe_2$ crystals through CVT method. (a) Schematic diagram of the experimental setup for the growth of $PtSe_2/PtTe_2$ crystals. (b) Top and side view of the crystal structure of 1T-$PtSe_2/PtTe_2$ (Blue: Pt, Green: Se/Te). (c) X-ray diffraction spectra of 1T-$PtSe_2/PtTe_2$ crystals (up) compared with the 1T-$PtSe_2/PtTe_2$ standard card of PDF#18−0970/PDF#18−0977 (bottom). Inset: the photograph of the synthesized $PtSe_2/PtTe_2$ crystals. (d) Raman spectra of $PtSe_2$ and $PtTe_2$ crystals.

Platinum dichalcogenide (PtX_2), a group-10 noble TMD, has been recently recognized as a remarkable candidate for the infrared photonic and optoelectronic applications owing to its environmental stability and unique layer-dependent electronic and optical properties.[27−33] Monolayer and bilayer $PtSe_2$ are predicted to have an indirect bandgap of ∼1.2 and ∼0.2 eV, respectively, while trilayer $PtSe_2$ and beyond have a zero-bandgap.[28,34] Similarly, monolayer $PtTe_2$ is predicted to possess an indirect bandgap of ∼0.4 eV, while bilayer $PtTe_2$ and beyond have a zero bandgap.[34] Recently, mechanically exfoliated bilayer $PtSe_2$ has been demonstrated as a photoactive material with a strong light absorption from visible to mid-IR range.[27] Interestingly, negative photoconduction is observed in ultrathin $PtSe_2$ film due to a photogating effect at Si/SiO_2 interface.[35] To further propel their practical application, a facile and scalable synthesis of 2D PtX_2 atomic flakes with controlled thickness is highly demanded. The current synthetic strategy mainly relies on chemical vapor deposition (CVD), or sonication-assisted liquid phase exfoliation (LPE) by probe sonication.[36−39] The mechanical exfoliation and chemical vapor deposition methods often yield multilayer structures, owing to their relatively larger interlayer binding energies as compared to other common TMD materials.[36,40−42] Sonication-assisted liquid phase exfoliation can produce few-layer PtX_2 flakes with small domain sizes that typically limit the performance of as-fabricated devices.[39] By contrast, a facile electrochemical exfoliation approach offers a rapid production of solution-processable few-layer 2D materials with micron lateral size at a large quantity and low cost.[17,43−46]

To this end, we report a facile electrochemical exfoliation approach for a rapid production of solution-processable high quality atomically thin $PtSe_2$ and $PtTe_2$ flakes. Bulky organic tetraalkylammonium (TAA) cations are used as the intercalant for the mild cathodic exfoliation of bulk $PtSe_2$ and $PtTe_2$ crystals to avoid the sample oxidation which would occur during the anodic exfoliation of 2D materials.[17,47,48] Under the optimized condition, bilayer $PtSe_2$ flakes can be readily exfoliated from bulk crystals with a yield of ∼44%. Furthermore, the photoresponse analysis based on as-exfoliated $PtSe_2$ and $PtTe_2$ bilayer flakes reveals outstanding performance with a high photoresponsivity of 72 mA W^{-1} and 1.62 A W^{-1} and decent specific detectivity of 1.44×10^9 and 2.11×10^9 Jones at zero gate voltage under the laser illumination of 1540 nm with a power density of 15.9 mW cm^{-2} and 0.16 W cm^{-2}, respectively.

RESULTS AND DISCUSSION

The Growth and Characterization of Bulk $PtSe_2$ and $PtTe_2$ Crystals. Figure 1a illustrates the growth process of the crystals in a quartz tube based on the chemical vapor transport (CVT) method (see details in the Experimental Section).[27,28,49] Representative PtX_2 single crystals with a lateral dimension of several mm are shown in the inset of Figure 1c. 1T-PtX_2 crystal possesses a typical hexagonal atomic structure under $P\bar{3}m1$ space group (Figure 1b).[27,30,50] X-ray diffraction (XRD) measurement of as-grown samples further confirms the crystal structure of $PtSe_2$ and $PtTe_2$ crystals (Figure 1c), consistent with the previous reports.[27,51] In addition, the presence of sharp peaks (001) indicates a good crystal quality of bulk $PtSe_2$ and $PtTe_2$ crystals. Raman spectrum acquired from the as-grown $PtSe_2$ ($PtTe_2$) crystals (Figure 1d) reveal two dominating features around 180 and 206.4 cm^{-1} (105.2 and 151.8 cm^{-1}), attributed to the E_g and the A_g modes corresponding to in-plane and out-of-plane phonon modes, respectively.[28,30,52,53] Therefore, both XRD data and Raman

https://dx.doi.org/10.1021/acsami.0c20535
ACS Appl. Mater. Interfaces 2021, 13, 8518−8527

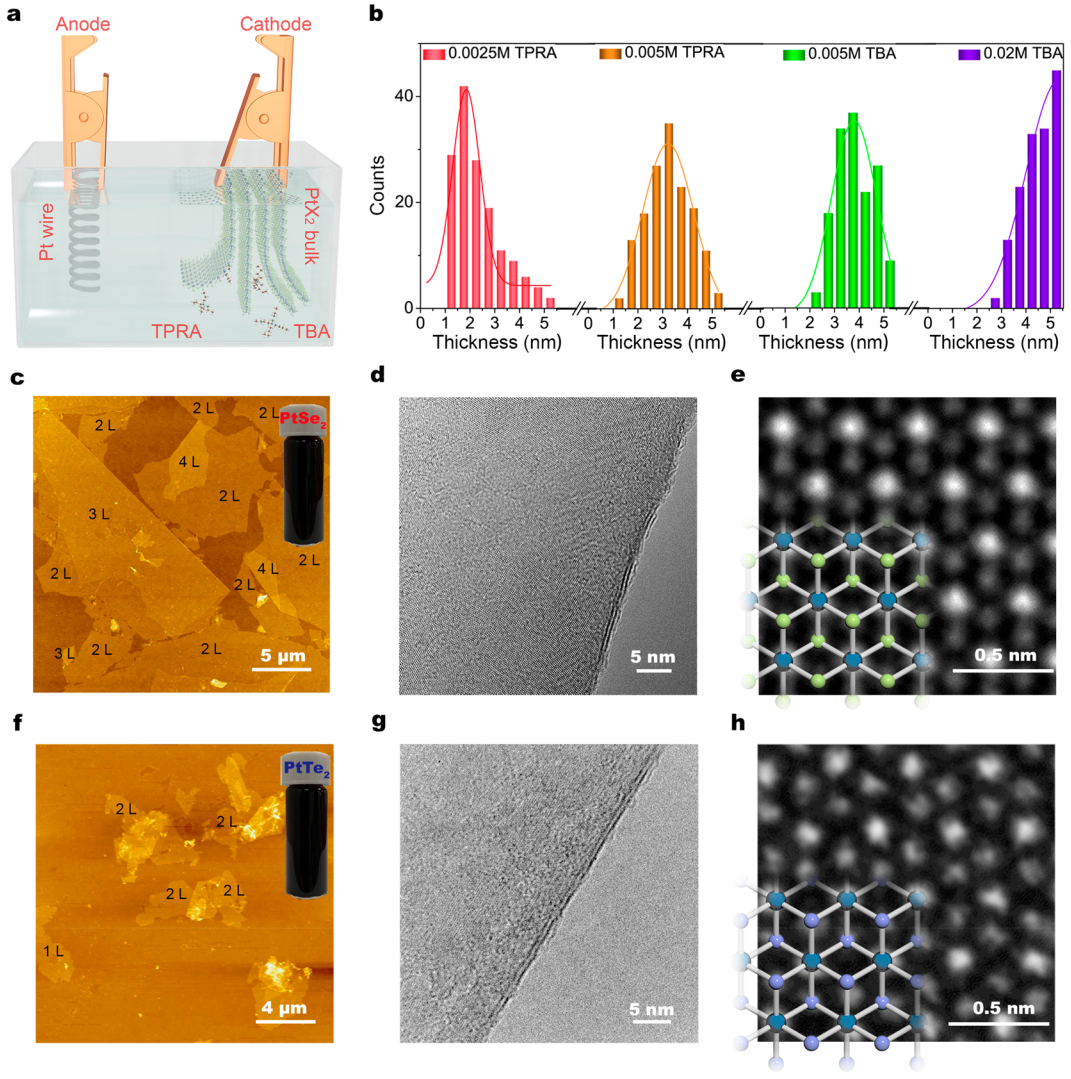

Figure 2. Characterization of the electrochemically exfoliated $PtSe_2/PtTe_2$ flakes. (a) Experimental setup for electrochemical exfoliation. (b) Statistics of the thickness of the $PtSe_2$ flakes exfoliated in DMSO solution under different conditions. (c,d) AFM image of the $PtSe_2$ (c) and $PtTe_2$ (f) flakes on SiO_2/Si substrate. The inset: photograph of the solution dispersion of exfoliated flakes. (d,e,g,h) TEM (d,g) and atomic resolution STEM-ADF (e,h) images of exfoliated $PtSe_2$ (d,e) and $PtTe_2$ (g,h).

spectrum demonstrate a good crystal quality of bulk $PtSe_2$ and $PtTe_2$.

The Electrochemical Exfoliation of $PtSe_2$ and $PtTe_2$ Bulk Crystals into Atomically Thin Flakes. Figure 2a illustrates the electrochemical exfoliation setup consisting of bulk $PtSe_2$ and $PtTe_2$ (cathode), Pt wire (anode), and organic TAA cations dissolved in dimethyl sulfoxide (DMSO) solvent (electrolyte).[17,54] It is noted that the thickness distribution of exfoliated $PtSe_2$ flakes can be controlled by tuning the length of alkyl chain of the TAA salts and their concentration as well as the solvent and cathodic voltage applied (Figure 2b). An optimal yield of bilayer $PtSe_2$ (~44%) can be achieved in electrolyte consisting of a 0.0025 M tetrapropylammonium (TPRA) in DMSO at the cathodic voltage of 6 V (refer to details in the Supporting Information (SI) Section 1 and Figure S2).[17] The thickness of the majority of as-exfoliated $PtSe_2/PtTe_2$ flakes is determined to be 1.2−1.5 nm by AFM imaging (Figure 2c,f and SI Figure S3), corresponding to the expected thickness of a bilayer $PtSe_2/PtTe_2$.[27] Raman spectra of different $PtSe_2$ and $PtTe_2$ flakes (SI Figure S4) reveal that E_g mode shows a blue shift when the flake becomes thinner.[39,50,52,53,55,56] The feature at ~230 cm^{-1} for bilayer-$PtSe_2$ flake is attributed to longitudinal optical (LO) modes.[52] The images of aberration-corrected scanning transmission electron microscopy−annular dark field (STEM-ADF) reveal a nearly perfect atomic crystal structure with each Pt atom (bright spot) surrounded by six dimmer Se/Te atoms, in agreement with the octahedral structure with the lattice constant of ~3.8 Å and ~4.0 Å expected for 1T-phase $PtSe_2$ and $PtTe_2$, respectively (Figure 2d,e,g,h).[27,51]

The Device Performance of a Bilayer $PtSe_2/PtTe_2$-Based Photodetector. As shown in Figure 3a−c, first-principles calculations predict the layer-dependent electronic structures of $PtSe_2$. Bilayer $PtSe_2$ possesses an indirect bandgap of ~0.23 eV, suitable for the infrared optoelectronics, in contrast to monolayer (an indirect bandgap of ~1.18 eV) and trilayer or above (semimetal).[34,57] We then fabricated a bilayer $PtSe_2$-based device to probe its photodetection performance in the IR regime (Figure 3g). The device adopts a typical field effect transistor configuration (Figure 3h) consisting of a heavily doped Si substrate as the back-gate and the Cr/Au (5 nm/60 nm) electrodes deposited by the electron-beam

https://dx.doi.org/10.1021/acsami.0c20535
ACS Appl. Mater. Interfaces 2021, 13, 8518−8527

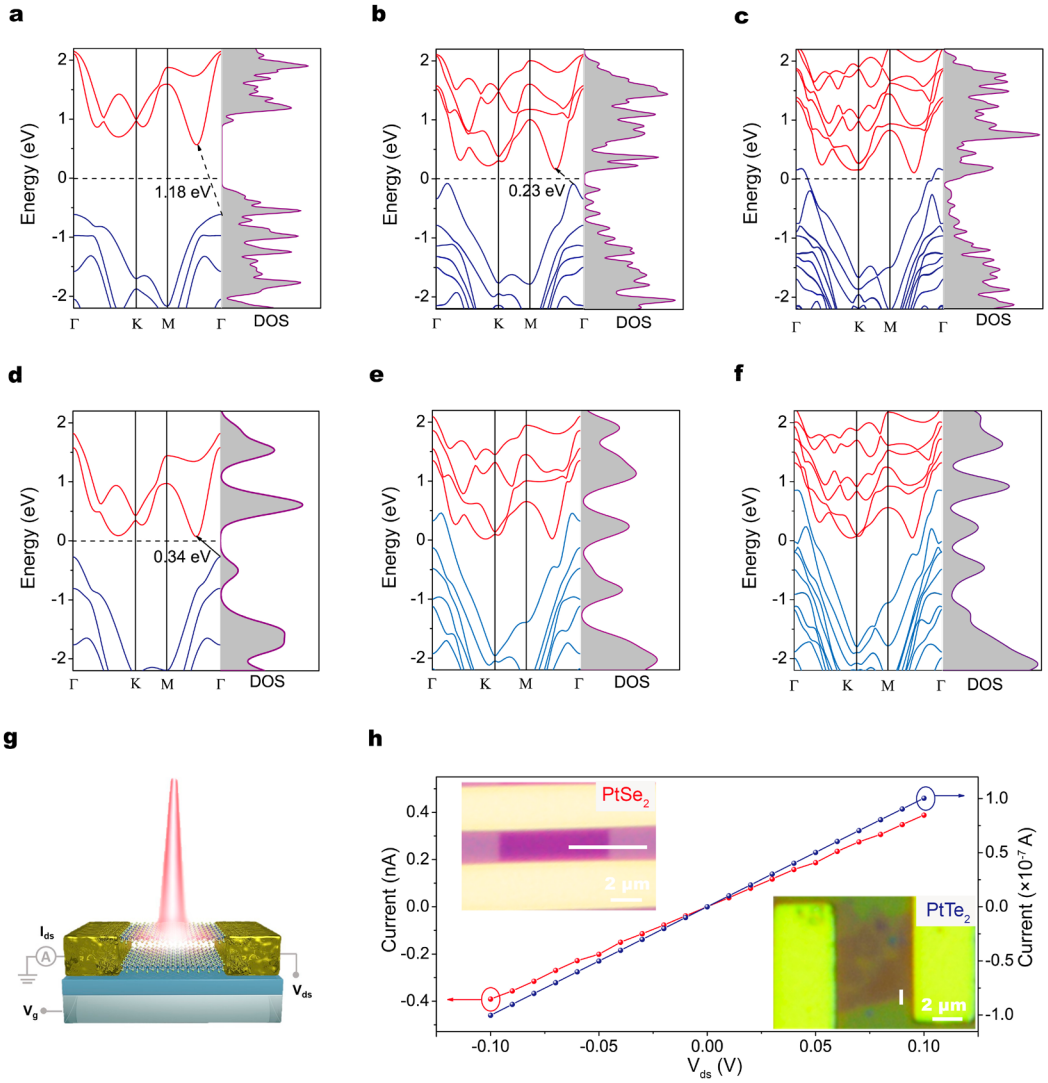

Figure 3. Theoretical calculations of band structure and density-of-states (DOS) of layered $PtSe_2$ and $PtTe_2$ and $I_{ds}-V_{ds}$ characteristics of bilayer-$PtSe_2$/$PtTe_2$ phototransistor devices. (a,b) Calculated band structure and DOS of (a) monolayer, (b) bilayer, and (c) trilayer $PtSe_2$ by first-principles calculations. (d–f) Calculated band structure and DOS of (d) monolayer, (e) bilayer, and (f) trilayer $PtTe_2$ by first-principles calculations. (g) Schematic diagram of the cross-section structure of the bilayer-$PtSe_2$/$PtTe_2$ device. (h) $I_{ds}-V_{ds}$ characteristics of the bilayer-$PtSe_2$/$PtTe_2$ FET under zero gate voltage and V_{ds} in the range of −0.1–0.1 V. Inset: Optical microscope images of the bilayer-$PtSe_2$/$PtTe_2$ devices.

evaporation. As depicted in Figure 3h, a linear $I_{ds}-V_{ds}$ curve measured in a small voltage range ($-0.1 < V_{ds} < 0.1$ V) implies an ohmic contact between bilayer $PtSe_2$ and metal electrodes. Furthermore, the contact resistance between the metal electrodes and the flake is determined to be $(5.8 \pm 0.5) \times 10^{-3}$ Ω cm^2 (SI Figure S5) according to the transmission line method (TLM).[58] The ohmic contact between the metal electrodes and the bilayer flake is beneficial for a high photodetection performance of bilayer $PtSe_2$-based device.[59]

Subsequently, the photodetection performance of a bilayer $PtSe_2$-based FET is investigated in the infrared region. First, the power density of a 1064 nm laser is modulated to record the photocurrent at V_{ds} = 0.5 V for the time-resolved photoresponse measurements as shown in Figure 4a (noted that $I_{ds}-V_{ds}$ characteristics are shown in SI Figure S6a). It is observed that the generated photocurrent (defined as $I_{ph} = I_{illum}-I_{dark}$) increases from ∼125 to ∼555 pA when the laser power density increases from 0.39 to 2.66 W cm^{-2} (Figure 4d and SI Figure S6a), which obeys a power law relationship($I_{ph} \propto P^{\alpha}$, where P is the incident power density).[14,27,60] The deviation from a linear relationship is possibly ascribed to the photogating dominated gain mechanism involving the generation, interaction, trapping and recombination of photocarriers.[10,24,61] Here, the power exponent α of the $PtSe_2$-based photodetector is extracted to be 0.781, consistent with the fact that low-dimensional materials-based photodetectors usually exhibit a power exponent α ranging from 0 to 1.[8,9,60]

The photoresponsivity and detectivity are considered as two important parameters for photodetectors.[14,27,60,62,63] The photoresponsivity and the detectivity can be defined using the following equations:[14,62,63]

$$R = \frac{I_{ph}}{P_{in}} \tag{1}$$

$$D^* = \frac{\sqrt{A}R}{\sqrt{2eI_d}} \tag{2}$$

where I_{ph}, P_{in}, A, e, I_d denote the photocurrent, the incident laser power, the effective device area, the electronic charge and

https://dx.doi.org/10.1021/acsami.0c20535
ACS Appl. Mater. Interfaces 2021, 13, 8518–8527

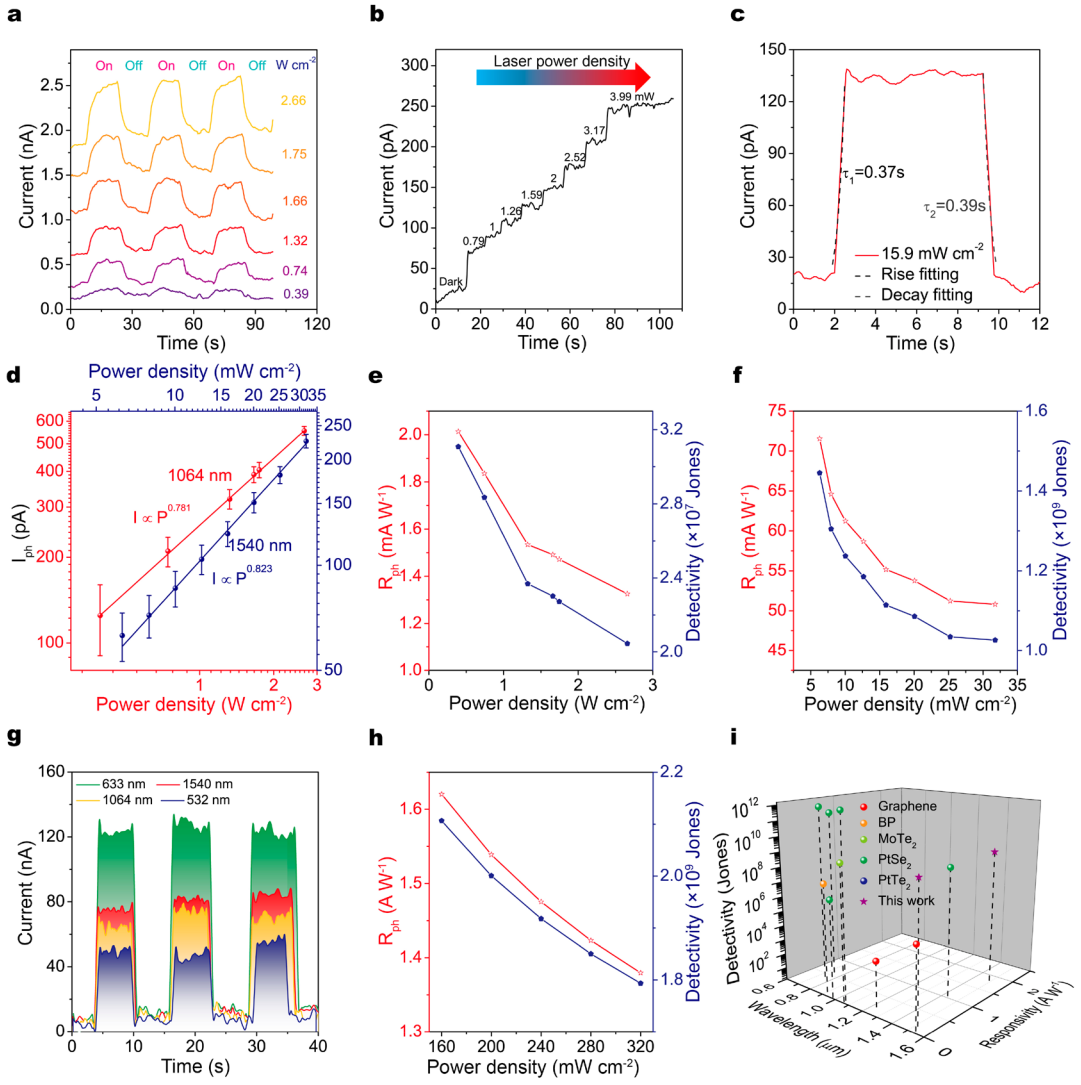

Figure 4. Optoelectronic properties of the bilayer-$PtSe_2$ and bilayer-$PtTe_2$ devices in the infrared region. (a,b) Time-resolved photocurrent of bilayer-$PtSe_2$ device for a bias voltage of 0.5 V and zero gate voltage excited by 1064 and 1540 nm laser illumination with different laser power density, respectively. (c) The rise and decay time of the photocurrent of bilayer-$PtSe_2$ device under the laser illumination with the wavelength of 1540 nm determined by fitting. (d) Power dependence of the photocurrent of the bilayer-$PtSe_2$ device recorded at V_{ds} = 0.5 V under 1064 and 1540 nm laser illumination. (e,f) Power dependence of the photoresponsivity and detectivity of the $PtSe_2$ device under 1064 and 1540 nm laser illumination, respectively. (g) Time-resolved photocurrent of bilayer-$PtTe_2$ device for a bias voltage of 0.5 V and zero gate voltage excited by 532 nm, 633 nm, 1064 nm, and 1540 nm laser illumination with a power density of 0.16 W cm^{-2}. (h) Power dependence of the photoresponsivity and detectivity of the $PtTe_2$ device under 1540 nm laser illumination. (i) Comparison with the reported infrared photodetector based on 2D materials.

the dark current, respectively. The laser power density dependent measurement reveals that both R and D^* decrease as the power density of incident laser increases (Figure 4e). The maximum of the photoresponsivity reaches 2 mA W^{-1} with a power density of 0.39 W cm^{-2}, much lower than other reported TMD-based photodetectors.[10,15,19] This is presumably due to a low light absorption coefficient at 1064 nm for the electrochemically exfoliated bilayer $PtSe_2$. The absorption measurement indeed reveals that the exfoliated $PtSe_2$ flakes exhibit a local absorption maximum between 1400 and 1600 nm (SI Figure S7 and S8), which suggests an increase of bandgap of the majority of bilayer flakes in the solution, presumably due to the presence of residual intercalated species in the interlayer space, consistent with the AFM height profile measured over bilayer flakes (SI Figure S9a). We then investigated the photodetection performance of the same device under the same laser power density (15.9 mW cm^{-2}) at the wavelength of 1540 nm, which reveals a dramatically enhanced photocurrent up to ~123 pA. Furthermore, the rise and decay time could be determined by fitting curves with the following equations:[64]

$$I_{rise} = I_0 + A_1 \exp\left(\frac{t - t_1}{\tau_1}\right) \quad (3)$$

$$I_{decay} = I_0 + A_2 \exp\left(-\frac{t - t_2}{\tau_2}\right) \quad (4)$$

where τ is the rise/decay time constant and t_1 or t_2 is the time of laser switching-on or switching-off, respectively. Here, τ_1 and τ_2 are determined to be ~0.37 s for rise time and ~0.39 s for decay time respectively (Figure 4c), superior to that at the wavelength of 1064 nm. In addition, the time period of the current range from 10% to 90% in rising and decaying is

https://dx.doi.org/10.1021/acsami.0c20535
ACS Appl. Mater. Interfaces 2021, 13, 8518−8527

determined to be ~0.38 s, consistent with the above fitted results (SI Figures S10 and S17 in Section 2). Figure 4d shows an apparent rise of the photocurrent against the laser power density. A standard fitting (based on $(I_{ph} \propto P^{\alpha})$ gives rise to a power exponent α of 0.823. This is probably due to the fact that high energy defect states cannot trap the photogenerated carriers at 1540 nm, leading to an enhanced photocurrent.[24,60] As depicted in Figure 4f, an increase of the incident laser power density reduces the photoresponsivity and detectivity, consistent with the previous report on other 2D materials based photodetectors.[29,60] The presence of trap states results in a higher carrier recombination rate under a larger laser power density, leading to a shorter average carrier lifetime and thus a lower photogain and photoresponsivity.[14,60] Moreover, the $PtSe_2$ device exhibits a high photoresponsivity of 72 mA W^{-1} under the laser power density of 6.29 mW cm^{-2} at 1540 nm, nearly 2 orders of magnitude higher than that at 1064 nm. Furthermore, as-fabricated $PtSe_2$ bilayer device shows a negligible decrease in the photocurrent after its storage in air for 3 months, suggesting a good stability (SI Figure S11). In addition, the structural anisotropy in $PtSe_2$ monolayer endows its properties with a polarization sensitive photodetection.[13,65] Indeed, the photocurrent varies with the change of polarization angle and reaches the maximum and minimum value at 0° and 90°, respectively (SI Figure S12). The linear dichroism properties of $PtSe_2$ will expand its potential application for future photonic and optoelectronic devices.

Apart from $PtSe_2$, monolayer $PtTe_2$ also possesses an indirect bandgap of ~0.34 eV, in contrast to bilayer and trilayer $PtTe_2$(zero bandgap). This suggests that $PtTe_2$ atomic layers may serve as another promising candidate for IR photodetection (Figure 3d–f and SI Figure S13).[66] Figure 3h shows a linear $I_{ds}-V_{ds}$ curve measured in a small voltage range $(-0.1<V_{ds} < 0.1\ V)$, implying an ohmic contact between bilayer $PtTe_2$ and metal electrodes in the bilayer-$PtTe_2$ device. Figure 4g shows that the bilayer-$PtTe_2$ photodetector demonstrates excellent photodetection performance in visible and infrared regime (SI Table S1). In detail, the bilayer-$PtTe_2$ device exhibits an excellent photoresponsivity of 1.62 A W^{-1} and the detectivity of 2.11×10^9 Jones under the laser power density of 0.16 W cm^{-2} at 1540 nm with excellent stability (Figure 4h and SI Figures S14 and S15). The photoresponsivity of bilayer-$PtTe_2$ device at 1540 nm is about 1 order of magnitude higher than that of bilayer-$PtSe_2$ device, while the detectivity of both devices lies in the same order of magnitude. The photoresponsivity and specific detectivity of the $PtSe_2$ and $PtTe_2$ devices in the IR regime is also superior or comparable to that of similar photodetectors made by graphene,[11,12] BP,[20] and TMD materials,[16,28,29,32,66,67] as shown in Figure 4i and SI Table S2. The photodetection performance of PtX_2-based photodetectors (e.g., rise/decay time and photoresponsivity) is comparable to that of the conventional IR photodetectors of PbS quantum dots (QDs).[68,69]

To further bridge the gap between the lab demonstration and practical applications, we utilize the high-solution processability of the exfoliated flakes to fabricate the large-scale and air-stable photodetectors on the quartz substrates. As shown in SI Figure S16a, the $PtSe_2$, and $PtTe_2$ thin film is deposited onto the substrate via drop-cast techniques. The time-resolved photoresponse measurement of the large-scale device (SI Figure S16) reveals that the photocurrent also increases, while the rise and decay time of the photoresponse decrease with an increase of the incident laser power. Furthermore, the large-scale photodetector shows a remarkable air-stability (>several months tested). However, the rise and decay time are much longer than that of the photodetector based on a single flake, which is presumably due to the weak penetrability of the infrared photons that influence the laser absorption of the underlying flakes.

CONCLUSIONS

In summary, a facile and general electrochemical approach is developed to exfoliate the $PtSe_2$ and $PtTe_2$ bulk crystals into high-quality atomically thin $PtSe_2$ and $PtTe_2$ flakes with a high bilayer yield under the optimized conditions. Furthermore, as-exfoliated bilayer $PtSe_2$ flake delivers an excellent photodetection performance with a high photoresponsivity of 0.072 A W^{-1} and the detectivity of 1.44×10^9 Jones at 1540 nm with a laser power density of 15.9 mW cm^{-2}, which can maintain its device performance more than 3 months. As-exfoliated $PtTe_2$ bilayer exhibits an excellent photoresponsivity of 1.62 A W^{-1} and the detectivity of 2.11×10^9 Jones at 1540 nm with a laser power density of 0.16 W cm^{-2}, about 4 orders of magnitude higher than the photoresponsivity of graphene-based device. In addition, the high solution-processability of exfoliated flakes allows for the fabrication of the large-scale $PtSe_2$ and $PtTe_2$ thin film devices with a high stability and a good photodetection performance. Therefore, this work offers a promising route for the scalable synthesis of air-stable PtX_2 atomic layers with controlled thickness for the superior photodetection performance in the IR regime under ambient conditions.

EXPERIMENTAL SECTION

Synthesis of $PtSe_2$ and $PtTe_2$ Crystals. The experimental set up shown in Figure 1a was used to grown bulk $PtSe_2$ though CVT method.[27,28,49] A mixture of Pt, Se, P, and S powders (the total weight of 350 mg) with a molar ratio of 1:2:1:3 plus iodine (17 mg, act as the transport gas) were sealed in a vacuum (10^{-6} Torr) quartz tube, which was placed into a muffle furnace subsequently. The temperature of the muffle furnace was fist kept at 900 °C for 40 h and then at 700 °C for 5 days. $PtSe_2$ bulk crystals are obtained after cooling to the room temperature. Bulk $PtTe_2$ crystal was also grown through CVT method. A mixture of Pt and Te powders with a molar ratio of 1:2.03 (the total weight is 301 mg) were sealed in quartz tube under the vacuum and put into the furnace. The temperature of the furnace was gradually increased to 1000 °C at the speed of 1 °C min^{-1} and kept at 1000 °C for 2 days, followed by a slow increase to 1150 °C (Kept for 60 min) at the speed of 1 °C min^{-1}. Finally, the furnace was cooled down to the room temperature at the speed of 1 °C min^{-1}.

Device Fabrication. Bulk $PtSe_2/PtTe_2$ crystals with typical dimensions of 2 × 2 × 1 mm^3 (length × width × thickness) were fixed on a Pt clip for a cathodic exfoliation at −6 V (vs Pt counter electrode) for 20 min (SI Figure S1). The bilayer yield was determined via AFM statistics. The bilayer yield was determined via the statistical analysis of the AFM height of as-exfoliated flakes. Specifically, exfoliated $PtSe_2/PtTe_2$ flakes in electrolyte were subjected to centrifugation at 3000 rpm (503.6 g) to separate them from unexfoliated bulks. The upper dispersion was dropped onto the SiO_2/Si substrates. We then measured the thickness of more than 150 individual flakes on the SiO_2/Si substrates by AFM imaging (SI Figure S2). The yield of bilayer flakes refers to the percentage of bilayer among all the flakes measured.[17] $PtSe_2/PtTe_2$ bilayer device: as-exfoliated $PtSe_2/PtTe_2$ flakes were first deposited onto the SiO_2/Si substrate via drop-casting and then were placed in DMSO to remove residual TAA salts and subsequently were dried in a vacuum tube. The target flakes were identified by the optical microscopy (Olympus BX51 microscope) and AFM (Park XE-100 system) imaging for device fabrications. After conducting the standard photolithography

https://dx.doi.org/10.1021/acsami.0c20535
ACS Appl. Mater. Interfaces 2021, 13, 8518−8527

procedures, we deposited Cr/Au (5 nm/60 nm) metal electrodes by the electron-beam evaporation method. Large-scale device fabrication: the exfoliated $PtSe_2/PtTe_2$ solution was subjected to centrifugation for 5 min at 3000 rpm (503.6 g) to remove thick unexfoliated flakes. The following two steps were repeated three times to remove the residual TAA salts in the exfoliated solution: (1) The solution was first centrifuged for 15 min at 12 000 rpm (8.057k g); (2) Remove the supernatant in the centrifuge tube and then shake the tube several times after adding the pure DMSO solvent. After the removal of the solvent via centrifugation, the concentrated $PtSe_2/PtTe_2$ inks can be obtained for large-scale device fabrication. Finally, Au (60 nm) electrodes were deposited by e-beam evaporation after placing a mask onto the $PtSe_2/PtTe_2$ flakes deposited on the quartz substrates.

Characterization. Optical images of the exfoliated $PtSe_2/PtTe_2$ flakes on the substrate were obtained via an Olympus BX51 microscope. XRD measurements of the grown bulk crystals were conducted by a Bruker X-ray diffractometer system. AFM (Park XE-100 system) was used to characterize the surface morphology and thickness of the $PtSe_2/PtTe_2$ flakes. An aberration-corrected ARM200F, equipped with a cold field-emission gun and an ASCOR corrector operating at 80 kV was utilized to obtain atomic-resolution STEM-ADF images. In addition, Raman spectra of the bulk crystals and exfoliated $PtSe_2/PtTe_2$ flakes were measured with a 532 nm laser excitation with the power of ~1 mW, 100× objective lens and a dispersive grating with 2400 l/mm at room temperature (WITec Alpha 300R Raman system). The absorption data of the exfoliated $PtSe_2$ flakes were collected using a UV−visible spectrophotometer. The photoresponse measurements of the $PtSe_2/PtTe_2$-based photodetector devices were conducted in the atmosphere with the illumination of different laser sources (a spot radius of 2 mm). The bias voltage across the channel and the drain-source current data were applied and collected respectively in a Keithley 4200 source meter system.

■ ASSOCIATED CONTENT

Supporting Information

The Supporting Information is available free of charge at https://pubs.acs.org/doi/10.1021/acsami.0c20535.

Additional information includes methods; electrochemical exfoliation current as the function of the applied electrochemical voltage; statistics histograms of the thickness of as-exfoliated $PtSe_2$ flakes; AFM image and line profiles of the $PtSe_2$ flakes on SiO_2/Si substrate; Raman spectra of few-layer and bulk $PtSe_2$ and $PtTe_2$, $I_{ds}-V_{ds}$ characteristics of the $PtSe_2$-based device, absorption spectrum of the $PtSe_2$ flakes from UV−visible spectrophotometer, photocurrent, and absorption results under laser illumination with different wavelength ranging from 1500 to 1600 nm; line profiles of $PtSe_2$ and $PtTe_2$ flakes; stability of bilayer-$PtSe_2$ device in atmospheric condition; linear polarization angle dependent photocurrent, UV−vis spectrum of as-exfoliated $PtTe_2$ flakes dispersed in DMSO; $I_{ds}-V_{ds}$ curves of the bilayer-$PtTe_2$ device; stability of bilayer-$PtTe_2$ device in atmospheric condition, photodetection performance of large-scale $PtSe_2$ and $PtTe_2$ devices, optoelectronic performance of $PtTe_2$-based device; optoelectronic performance of $PtTe_2$-based photodetector under the laser of various wavelength; a list of 2D materials based infrared photodetectors (PDF)

■ AUTHOR INFORMATION

Corresponding Authors

Jiong Lu − *Department of Chemistry and Centre for Advanced 2D Materials and Graphene Research Centre, National University of Singapore, Singapore 117543, Singapore;* orcid.org/0000-0002-3690-8235; Email: chmluj@nus.edu.sg

Ying Li − *SZU-NUS Collaborative Innovation Center for Optoelectronic Science & Technology, International Collaborative Laboratory of 2D Materials for Optoelectronics Science and Technology of Ministry of Education, College of Optoelectronic Engineering, Shenzhen University, Shenzhen 518060, China*; Email: queenly@szu.edu.cn

Jing Li − *Department of Chemistry and Centre for Advanced 2D Materials and Graphene Research Centre, National University of Singapore, Singapore 117543, Singapore;* orcid.org/0000-0002-5627-4153; Email: c2dlij@nus.edu.sg

Kedong Wang − *Department of Physics, Southern University of Science and Technology, Shenzhen 518055, China;* orcid.org/0000-0003-1253-5603; Email: wangkd@sustech.edu.cn

Authors

Yaping Ma − *SZU-NUS Collaborative Innovation Center for Optoelectronic Science & Technology, International Collaborative Laboratory of 2D Materials for Optoelectronics Science and Technology of Ministry of Education, College of Optoelectronic Engineering, Shenzhen University, Shenzhen 518060, China; Department of Chemistry, National University of Singapore, Singapore 117543, Singapore;* orcid.org/0000-0003-3907-6881

Xiji Shao − *Department of Physics, Southern University of Science and Technology, Shenzhen 518055, China*

Bowei Dong − *Department of Electrical and Computer Engineering, National University of Singapore, Singapore 117576, Singapore*

Zhenliang Hu − *Department of Physics, National University of Singapore, Singapore 117551, Singapore*

Qiulan Zhou − *Key Laboratory of Mesoscopic Chemistry, School of Chemistry and Chemical Engineering, Nanjing University, Nanjing 210023, China*

Haomin Xu − *Department of Chemistry, National University of Singapore, Singapore 117543, Singapore;* orcid.org/0000-0003-3704-1810

Xiaoxu Zhao − *Department of Materials Science and Engineering, National University of Singapore, Singapore 117575, Singapore*

Hanyan Fang − *Department of Chemistry, National University of Singapore, Singapore 117543, Singapore*

Xinzhe Li − *Department of Chemistry, National University of Singapore, Singapore 117543, Singapore;* orcid.org/0000-0001-6636-0496

Zejun Li − *Department of Chemistry, National University of Singapore, Singapore 117543, Singapore;* orcid.org/0000-0002-7582-0674

Jing Wu − *Centre for Advanced 2D Materials and Graphene Research Centre, National University of Singapore, Singapore 117546, Singapore; Institute of Materials Research and Engineering, Agency for Science, Technology and Research (A*STAR), Sigapore 138634, Singapore*

Meng Zhao − *Institute of Materials Research and Engineering, Agency for Science, Technology and Research (A*STAR), Sigapore 138634, Singapore*

Stephen John Pennycook − *Department of Materials Science and Engineering, National University of Singapore, Singapore 117575, Singapore*

https://dx.doi.org/10.1021/acsami.0c20535
ACS Appl. Mater. Interfaces 2021, 13, 8518−8527

Chorng Haur Sow − *Department of Physics, National University of Singapore, Singapore 117551, Singapore;* orcid.org/0000-0001-6385-3017

Chengkuo Lee − *Department of Electrical and Computer Engineering, National University of Singapore, Singapore 117576, Singapore;* orcid.org/0000-0002-8886-3649

Yu Lin Zhong − *Centre for Clean Environment and Energy, School of Environment and Science, Griffith University, Gold Coast, Queensland 4222, Australia;* orcid.org/0000-0001-6741-3609

Junpeng Lu − *School of Physics, Southeast University, Nanjing 211189, China;* orcid.org/0000-0002-7099-3162

Mengning Ding − *Key Laboratory of Mesoscopic Chemistry, School of Chemistry and Chemical Engineering, Nanjing University, Nanjing 210023, China;* orcid.org/0000-0001-6581-3385

Complete contact information is available at: https://pubs.acs.org/10.1021/acsami.0c20535

Author Contributions

J.Lu supervised the project. Y.M., Q.Z., and J.L. performed the sample growth and device fabrications. Y.M., J.L., B.D., and Z.H. performed photodetection performance measurements. Y.M. and H.F. performed AFM measurements. H.X. and X.Z. performed TEM characterization. X.S. and K.W. contributed to the first-principles calculations. Y.M. and J.L. wrote the paper. All authors took part in the discussion and preparation of the manuscript.

Notes

The authors declare no competing financial interest.

■ ACKNOWLEDGMENTS

J.L. acknowledges the support from MOE Tier 2 grant (MOE2019-T2-2-044 and R-143-000-A75-114) and NAMIC grant (R-143-000- B26-529). Y.M. acknowledges the financial support from the China Postdoctoral Science Foundation (2019M663033). J.L. acknowledges the support from the National Natural Science Foundation of China (21703143). K. Wang acknowledges the support from the General Physics Teaching Steering Committee of the Ministry of Education of China (Teaching Reform Project DJZW201931zn). M.Z. acknowledges the support from the Agency for Science, Technology and Research (A*STAR) (152700014 and H19H6a0025). Y.L.Z. acknowledges the support from the Australian Research Council (DP190100120). S.J.P. is grateful to the support from MOE Tier 2 grant (MOE2017-T2-2-139).

■ REFERENCES

(1) Sun, Y.; Gao, S.; Xie, Y. Atomically-Thick Two-Dimensional Crystals: Electronic Structure Regulation and Energy Device Construction. *Chem. Soc. Rev.* **2014**, *43*, 530−546.

(2) Hu, D.; Zhao, T.; Ping, X.; Zheng, H.; Xing, L.; Liu, X.; Zheng, J.; Sun, L.; Gu, L.; Tao, C. Unveiling the Layer-Dependent Catalytic Activity of $PtSe_2$ Atomic Crystals for the Hydrogen Evolution Reaction. *Angew. Chem.* **2019**, *131*, 7051−7055.

(3) Chang, K.; Mei, Z.; Wang, T.; Kang, Q.; Ouyang, S.; Ye, J. MoS_2/Graphene Cocatalyst for Efficient Photocatalytic H_2 Evolution under Visible Light Irradiation. *ACS Nano* **2014**, *8*, 7078−7087.

(4) Tsai, M.-L.; Su, S.-H.; Chang, J.-K.; Tsai, D.-S.; Chen, C.-H.; Wu, C.-I.; Li, L.-J.; Chen, L.-J.; He, J.-H. Monolayer MoS_2 Heterojunction Solar Cells. *ACS Nano* **2014**, *8*, 8317−8322.

(5) Jiang, H.; Ren, D.; Wang, H.; Hu, Y.; Guo, S.; Yuan, H.; Hu, P.; Zhang, L.; Li, C. 2D Monolayer MoS_2-Carbon Interoverlapped Superstructure: Engineering Ideal Atomic Interface for Lithium Ion Storage. *Adv. Mater.* **2015**, *27*, 3687−3695.

(6) Bie, Y.-Q.; Grosso, G.; Heuck, M.; Furchi, M. M.; Cao, Y.; Zheng, J.; Bunandar, D.; Navarro-Moratalla, E.; Zhou, L.; Efetov, D. K. A $MoTe_2$-based Light-Emitting Diode and Photodetector for Silicon Photonic Integrated Circuits. *Nat. Nanotechnol.* **2017**, *12*, 1124−1129.

(7) Michel, J.; Liu, J.; Kimerling, L. C. High-Performance Ge-on-Si Photodetectors. *Nat. Photonics* **2010**, *4*, 527−534.

(8) Konstantatos, G.; Badioli, M.; Gaudreau, L.; Osmond, J.; Bernechea, M.; De Arquer, F. P. G.; Gatti, F.; Koppens, F. H. Hybrid Graphene-Quantum dot Phototransistors with Ultrahigh Gain. *Nat. Nanotechnol.* **2012**, *7*, 363−368.

(9) Du, S.; Lu, W.; Ali, A.; Zhao, P.; Shehzad, K.; Guo, H.; Ma, L.; Liu, X.; Pi, X.; Wang, P. A Broadband Fluorographene Photodetector. *Adv. Mater.* **2017**, *29*, 1700463.

(10) Zhang, Y.; Liu, T.; Meng, B.; Li, X.; Liang, G.; Hu, X.; Wang, Q. J. Broadband High Photoresponse from Pure Monolayer Graphene Photodetector. *Nat. Commun.* **2013**, *4*, 1−11.

(11) Xia, F.; Mueller, T.; Lin, Y.-M.; Valdes-Garcia, A.; Avouris, P. Ultrafast Graphene Photodetector. *Nat. Nanotechnol.* **2009**, *4*, 839−843.

(12) Mueller, T.; Xia, F.; Avouris, P. Graphene Photodetectors for High-Speed Optical Communications. *Nat. Photonics* **2010**, *4*, 297−301.

(13) Zhang, E.; Wang, P.; Li, Z.; Wang, H.; Song, C.; Huang, C.; Chen, Z.-G.; Yang, L.; Zhang, K.; Lu, S. Tunable Ambipolar Polarization-Sensitive Photodetectors based on High-Anisotropy $ReSe_2$ Nanosheets. *ACS Nano* **2016**, *10*, 8067−8077.

(14) Zeng, L. H.; Wu, D.; Lin, S. H.; Xie, C.; Yuan, H. Y.; Lu, W.; Lau, S. P.; Chai, Y.; Luo, L. B.; Li, Z. J. Controlled Synthesis of 2D Palladium Diselenide for Sensitive Photodetector Applications. *Adv. Funct. Mater.* **2019**, *29*, 1806878.

(15) Wang, W.; Klots, A.; Prasai, D.; Yang, Y.; Bolotin, K. I.; Valentine, J. Hot Electron-based Near-infrared Photodetection using Bilayer MoS_2. *Nano Lett.* **2015**, *15*, 7440−7444.

(16) Huang, H.; Wang, J.; Hu, W.; Liao, L.; Wang, P.; Wang, X.; Gong, F.; Chen, Y.; Wu, G.; Luo, W. Highly Sensitive Visible to Infrared MoTe2 Photodetectors Enhanced by the Photogating Effect. *Nanotechnology* **2016**, *27*, 445201.

(17) Li, J.; Chen, C.; Liu, S.; Lu, J.; Goh, W. P.; Fang, H.; Qiu, Z.; Tian, B.; Chen, Z.; Yao, C. Ultrafast Electrochemical Expansion of Black Phosphorus toward High-yield Synthesis of Few-layer Phosphorene. *Chem. Mater.* **2018**, *30*, 2742−2749.

(18) Yuan, H.; Liu, X.; Afshinmanesh, F.; Li, W.; Xu, G.; Sun, J.; Lian, B.; Curto, A. G.; Ye, G.; Hikita, Y. Polarization-Sensitive Broadband Photodetector using a Black Phosphorus Vertical p-n Junction. *Nat. Nanotechnol.* **2015**, *10*, 707−713.

(19) Guo, Q.; Pospischil, A.; Bhuiyan, M.; Jiang, H.; Tian, H.; Farmer, D.; Deng, B.; Li, C.; Han, S.-J.; Wang, H. Black Phosphorus Mid-infrared Photodetectors with High Gain. *Nano Lett.* **2016**, *16*, 4648−4655.

(20) Buscema, M.; Groenendijk, D. J.; Blanter, S. I.; Steele, G. A.; Van Der Zant, H. S.; Castellanos-Gomez, A. Fast and Broadband Photoresponse of Few-Layer Black Phosphorus Field-Effect Transistors. *Nano Lett.* **2014**, *14*, 3347−3352.

(21) Sun, Z.; Chang, H. Graphene and Graphene-like Two-Dimensional Materials in Photodetection: Mechanisms and Methodology. *ACS Nano* **2014**, *8*, 4133−4156.

(22) Zhang, Q.; Jie, J.; Diao, S.; Shao, Z.; Zhang, Q.; Wang, L.; Deng, W.; Hu, W.; Xia, H.; Yuan, X. Solution-Processed Graphene Quantum Dot Deep-UV Photodetectors. *ACS Nano* **2015**, *9*, 1561−1570.

(23) Di Bartolomeo, A. Graphene Schottky Diodes: An Experimental Review of the Rectifying Graphene/Semiconductor Heterojunction. *Phys. Rep.* **2016**, *606*, 1−58.

(24) Koppens, F.; Mueller, T.; Avouris, P.; Ferrari, A.; Vitiello, M.; Polini, M. Photodetectors based on Graphene, Other Two-Dimen-

sional Materials and Hybrid Systems. *Nat. Nanotechnol.* **2014**, *9*, 780−793.
(25) Ye, L.; Li, H.; Chen, Z.; Xu, J. Near-infrared Photodetector based on MoS_2/Black Phosphorus Heterojunction. *ACS Photonics* **2016**, *3*, 692−699.
(26) Yin, J.; Tan, Z.; Hong, H.; Wu, J.; Yuan, H.; Liu, Y.; Chen, C.; Tan, C.; Yao, F.; Li, T. Ultrafast and Highly Sensitive Infrared Photodetectors based on Two-Dimensional Oxyselenide Crystals. *Nat. Commun.* **2018**, *9*, 1−7.
(27) Yu, X.; Yu, P.; Wu, D.; Singh, B.; Zeng, Q.; Lin, H.; Zhou, W.; Lin, J.; Suenaga, K.; Liu, Z. Atomically Thin Noble Metal Dichalcogenide: a Broadband Mid-infrared Semiconductor. *Nat. Commun.* **2018**, *9*, 1−9.
(28) Zhao, Y.; Qiao, J.; Yu, Z.; Yu, P.; Xu, K.; Lau, S. P.; Zhou, W.; Liu, Z.; Wang, X.; Ji, W. High-electron-mobility and Air-stable 2D Layered $PtSe_2$ FETs. *Adv. Mater.* **2017**, *29*, 1604230.
(29) Zeng, L. H.; Lin, S. H.; Li, Z. J.; Zhang, Z. X.; Zhang, T. F.; Xie, C.; Mak, C. H.; Chai, Y.; Lau, S. P.; Luo, L. B. Fast, Self-driven, Air-Stable, and Broadband Photodetector based on Vertically Aligned $PtSe_2$/GaAs Heterojunction. *Adv. Funct. Mater.* **2018**, *28*, 1705970.
(30) Zeng, L.; Lin, S.; Lou, Z.; Yuan, H.; Long, H.; Li, Y.; Lu, W.; Lau, S. P.; Wu, D.; Tsang, Y. H. Ultrafast and Sensitive Photodetector based on a $PtSe_2$/Silicon Nanowire Array Heterojunction with a Multiband Spectral Response from 200 to 1550 nm. *NPG Asia Mater.* **2018**, *10*, 352−362.
(31) Yim, C.; McEvoy, N.; Riazimehr, S.; Schneider, D. S.; Gity, F.; Monaghan, S.; Hurley, P. K.; Lemme, M. C.; Duesberg, G. S. Wide Spectral Photoresponse of Layered Platinum Diselenide-based Photodiodes. *Nano Lett.* **2018**, *18*, 1794−1800.
(32) Wu, D.; Wang, Y.; Zeng, L.; Jia, C.; Wu, E.; Xu, T.; Shi, Z.; Tian, Y.; Li, X.; Tsang, Y. H. Design of 2D Layered $PtSe_2$ Heterojunction for the High-Performance, Room-Temperature, Broadband, Infrared Photodetector. *ACS Photonics* **2018**, *5*, 3820−3827.
(33) Zhuo, R.; Zeng, L.; Yuan, H.; Wu, D.; Wang, Y.; Shi, Z.; Xu, T.; Tian, Y.; Li, X.; Tsang, Y. H. In-situ Fabrication of $PtSe_2$/GaN Heterojunction for Self-Powered Deep Ultraviolet Photodetector with Ultrahigh Current on/off Ratio and Detectivity. *Nano Res.* **2019**, *12*, 183−189.
(34) Villaos, R. A. B.; Crisostomo, C. P.; Huang, Z.-Q.; Huang, S.-M.; Padama, A. A. B.; Albao, M. A.; Lin, H.; Chuang, F.-C. Thickness Dependent Electronic Properties of Pt Dichalcogenides. *npj 2D Materials and Applications* **2019**, *3*, 1−8.
(35) Urban, F.; Gity, F.; Hurley, P. K.; McEvoy, N.; Di Bartolomeo, A. Isotropic Conduction and Negative Photoconduction in Ultrathin $PtSe_2$ Films. *Appl. Phys. Lett.* **2020**, *117*, 193102.
(36) Shawkat, M. S.; Chung, H.-S.; Dev, D.; Das, S.; Roy, T.; Jung, Y. Two-Dimensional/Three-Dimensional Schottky Junction Photovoltaic Devices Realized by the Direct CVD Growth of vdW 2D $PtSe_2$ Layers on Silicon. *ACS Appl. Mater. Interfaces* **2019**, *11*, 27251−27258.
(37) Wang, Z.; Li, Q.; Besenbacher, F.; Dong, M. Facile Synthesis of Single Crystal $PtSe_2$ Nanosheets for Nanoscale Electronics. *Adv. Mater.* **2016**, *28*, 10224−10229.
(38) Wang, Y.; Li, L.; Yao, W.; Song, S.; Sun, J.; Pan, J.; Ren, X.; Li, C.; Okunishi, E.; Wang, Y.-Q. Monolayer $PtSe_2$, a New Semiconducting Transition-Metal-Dichalcogenide, Epitaxially Grown by Direct Selenization of Pt. *Nano Lett.* **2015**, *15*, 4013−4018.
(39) Szydłowska, B. M.; Hartwig, O.; Tywoniuk, B.; Hartman, T.; Stimpel-Lindner, T.; Sofer, Z.; McEvoy, N.; Duesberg, G. S.; Backes, C. Spectroscopic Thickness and Quality Metrics for $PtSe_2$ Layers Produced by Topdown and Bottom-up Techniques. *2D Mater.* **2020**, *7*, 045027.
(40) Han, S. S.; Kim, J. H.; Noh, C.; Kim, J. H.; Ji, E.; Kwon, J.; Yu, S. M.; Ko, T.-J.; Okogbue, E.; Oh, K. H. Horizontal-to-Vertical Transition of 2D Layer Orientation in Low-Temperature Chemical Vapor Deposition-Grown $PtSe_2$ and Its Influences on Electrical Properties and Device Applications. *ACS Appl. Mater. Interfaces* **2019**, *11*, 13598−13607.
(41) Mounet, N.; Gibertini, M.; Schwaller, P.; Campi, D.; Merkys, A.; Marrazzo, A.; Sohier, T.; Castelli, I. E.; Cepellotti, A.; Pizzi, G. Two-Dimensional Materials from High-Throughput Computational Exfoliation of Experimentally Known Compounds. *Nat. Nanotechnol.* **2018**, *13*, 246−252.
(42) Kempt, R.; Kuc, A.; Heine, T. Two-Dimensional Noble-Metal Chalcogenides and Phosphochalcogenides. *Angew. Chem., Int. Ed.* **2020**, *59*, 9242−9254.
(43) Lu, J.; Yang, J.-X.; Wang, J.; Lim, A.; Wang, S.; Loh, K. P. One-Pot Synthesis of Fluorescent Carbon Nanoribbons, Nanoparticles, and Graphene by the Exfoliation of Graphite in Ionic Liquids. *ACS Nano* **2009**, *3*, 2367−2375.
(44) Parvez, K.; Wu, Z.-S.; Li, R.; Liu, X.; Graf, R.; Feng, X.; Mullen, K. Exfoliation of Graphite into Graphene in Aqueous Solutions of Inorganic Salts. *J. Am. Chem. Soc.* **2014**, *136*, 6083−6091.
(45) Abdelkader, A.; Cooper, A.; Dryfe, R.; Kinloch, I. How to Get between the Sheets: a Review of Recent Works on the Electrochemical Exfoliation of Graphene Materials from Bulk Graphite. *Nanoscale* **2015**, *7*, 6944−6956.
(46) Li, J.; Song, P.; Zhao, J.; Vaklinova, K.; Zhao, X.; Li, Z.; Qiu, Z.; Wang, Z.; Lin, L.; Zhao, M. Printable Two-Dimensional Superconducting Monolayers. *Nat. Mater.* **2021**, *20*, 1−7.
(47) Fang, Y.; Li, X.; Li, J.; Yao, C.; Hoh, H. Y.; Hai, X.; Lu, J.; Su, C. Janus Electrochemical Exfoliation of Two-Dimensional Materials. *J. Mater. Chem. A* **2019**, *7*, 25691−25711.
(48) Yang, S.; Zhang, P.; Nia, A. S.; Feng, X. Emerging 2D Materials Produced via Electrochemistry. *Adv. Mater.* **2020**, *32*, 1907857.
(49) Soled, S.; Wold, A.; Gorochov, O. Crystal Growth and Characterization of Several Platinum Sulfoselenides. *Mater. Res. Bull.* **1976**, *11*, 927−932.
(50) Yim, C.; Lee, K.; McEvoy, N.; O'Brien, M.; Riazimehr, S.; Berner, N. C.; Cullen, C. P.; Kotakoski, J.; Meyer, J. C.; Lemme, M. C. High-Performance Hybrid Electronic Devices from Layered $PtSe_2$ Films Grown at Low Temperature. *ACS Nano* **2016**, *10*, 9550−9558.
(51) Yan, M.; Wang, E.; Zhou, X.; Zhang, G.; Zhang, H.; Zhang, K.; Yao, W.; Lu, N.; Yang, S.; Wu, S. High Quality Atomically Thin $PtSe_2$ Films Grown by Molecular Beam Epitaxy. *2D Mater.* **2017**, *4*, 045015.
(52) O'Brien, M.; McEvoy, N.; Motta, C.; Zheng, J.-Y.; Berner, N. C.; Kotakoski, J.; Elibol, K.; Pennycook, T. J.; Meyer, J. C.; Yim, C. Raman Characterization of Platinum Diselenide Thin Films. *2D Mater.* **2016**, *3*, 021004.
(53) Yan, M.; Huang, H.; Zhang, K.; Wang, E.; Yao, W.; Deng, K.; Wan, G.; Zhang, H.; Arita, M.; Yang, H. Lorentz-violating Type-II Dirac Fermions in Transition Metal Dichalcogenide $PtTe_2$. *Nat. Commun.* **2017**, *8*, 1−6.
(54) Wang, C.; He, Q.; Halim, U.; Liu, Y.; Zhu, E.; Lin, Z.; Xiao, H.; Duan, X.; Feng, Z.; Cheng, R. Monolayer Atomic Crystal Molecular Superlattices. *Nature* **2018**, *555*, 231−236.
(55) Lee, C.; Yan, H.; Brus, L. E.; Heinz, T. F.; Hone, J.; Ryu, S. Anomalous Lattice Vibrations of Single-and Few-Layer MoS_2. *ACS Nano* **2010**, *4*, 2695−2700.
(56) Ma, H.; Chen, P.; Li, B.; Li, J.; Ai, R.; Zhang, Z.; Sun, G.; Yao, K.; Lin, Z.; Zhao, B. Thickness-Tunable Synthesis of Ultrathin Type-II Dirac Semimetal $PtTe_2$ Single Crystals and Their Thickness-Dependent Electronic Properties. *Nano Lett.* **2018**, *18*, 3523−3529.
(57) Ciarrocchi, A.; Avsar, A.; Ovchinnikov, D.; Kis, A. Thickness-Modulated Metal-to-Semiconductor Transformation in a Transition Metal Dichalcogenide. *Nat. Commun.* **2018**, *9*, 1−6.
(58) Wang, Y.; Kim, J. C.; Wu, R. J.; Martinez, J.; Song, X.; Yang, J.; Zhao, F.; Mkhoyan, A.; Jeong, H. Y.; Chhowalla, M. Van der Waals Contacts between Three-Dimensional Metals and Two-Dimensional Semiconductors. *Nature* **2019**, *568*, 70−74.
(59) Di Bartolomeo, A.; Pelella, A.; Liu, X.; Miao, F.; Passacantando, M.; Giubileo, F.; Grillo, A.; Iemmo, L.; Urban, F.; Liang, S. J. Pressure-Tunable Ambipolar Conduction and Hysteresis in Thin Palladium Diselenide Field Effect Transistors. *Adv. Funct. Mater.* **2019**, *29*, 1902483.
(60) Liang, Q.; Wang, Q.; Zhang, Q.; Wei, J.; Lim, S. X.; Zhu, R.; Hu, J.; Wei, W.; Lee, C.; Sow, C. High-Performance, Room

https://dx.doi.org/10.1021/acsami.0c20535
ACS Appl. Mater. Interfaces 2021, 13, 8518−8527

Temperature, Ultra-Broadband Photodetectors Based on Air-Stable $PdSe_2$. *Adv. Mater.* **2019**, *31*, 1807609.
(61) Urban, F.; Martucciello, N.; Peters, L.; McEvoy, N.; Di Bartolomeo, A. Environmental Effects on the Electrical Characteristics of Back-Gated WSe_2 Field-Effect Transistors. *Nanomaterials* **2018**, *8*, 901.
(62) Mao, J.; Yu, Y.; Wang, L.; Zhang, X.; Wang, Y.; Shao, Z.; Jie, J. Ultrafast, Broadband Photodetector based on MoSe2/Silicon Heterojunction with Vertically Standing Layered Structure using Graphene as Transparent Electrode. *Adv. Sci.* **2016**, *3*, 1600018.
(63) Choi, M. S.; Qu, D.; Lee, D.; Liu, X.; Watanabe, K.; Taniguchi, T.; Yoo, W. J. Lateral MoS_2 p-n Junction formed by Chemical Doping for Use in High-Performance Optoelectronics. *ACS Nano* **2014**, *8*, 9332−9340.
(64) Island, J. O.; Buscema, M.; Barawi, M.; Clamagirand, J. M.; Ares, J. R.; Sánchez, C.; Ferrer, I. J.; Steele, G. A.; van der Zant, H. S.; Castellanos-Gomez, A. Ultrahigh Photoresponse of Few-Layer TiS_3 Nanoribbon Transistors. *Adv. Opt. Mater.* **2014**, *2*, 641−645.
(65) Yang, Y.; Liu, S.-C.; Yang, W.; Li, Z.; Wang, Y.; Wang, X.; Zhang, S.; Zhang, Y.; Long, M.; Zhang, G. Air-stable In-plane Anisotropic GeSe2 for Highly Polarization-Sensitive Photodetection in Short Wave Region. *J. Am. Chem. Soc.* **2018**, *140*, 4150−4156.
(66) Xu, H.; Guo, C.; Zhang, J.; Guo, W.; Kuo, C. N.; Lue, C. S.; Hu, W.; Wang, L.; Chen, G.; Politano, A. $PtTe_2$-Based Type-II Dirac Semimetal and Its van der Waals Heterostructure for Sensitive Room Temperature Terahertz Photodetection. *Small* **2019**, *15*, 1903362.
(67) Zhang, Z.-X.; Zeng, L.-H.; Tong, X.-W.; Gao, Y.; Xie, C.; Tsang, Y. H.; Luo, L.-B.; Wu, Y.-C. Ultrafast, Self-driven, and Air-stable Photodetectors based on Multilayer $PtSe_2$/Perovskite Heterojunctions. *J. Phys. Chem. Lett.* **2018**, *9*, 1185−1194.
(68) Wei, Y.; Ren, Z.; Zhang, A.; Mao, P.; Li, H.; Zhong, X.; Li, W.; Yang, S.; Wang, J. Hybrid organic/PbS Quantum Dot Bilayer Photodetector with Low Dark Current and High Detectivity. *Adv. Funct. Mater.* **2018**, *28*, 1706690.
(69) Ren, Z.; Sun, J.; Li, H.; Mao, P.; Wei, Y.; Zhong, X.; Hu, J.; Yang, S.; Wang, J. Bilayer PbS Quantum Dots for High-Performance Photodetectors. *Adv. Mater.* **2017**, *29*, 1702055.

https://dx.doi.org/10.1021/acsami.0c20535
ACS Appl. Mater. Interfaces 2021, 13, 8518−8527